Synthesis, Crystal Structure, and Thermal Properties of a Holmium(III) Benzoate Complex with 1,10-Phenanthroline

Juan-Fen Wang,[†,‡] Ning Ren,[§] Jian-Jun Zhang,*[,†,‡] Ke-Zhong Wu,[‡] and Shu-Ping Wang[‡]

Experimental Center, Hebei Normal University, Shijiazhuang 050016, P. R. China, College of Chemistry & Material Science, Hebei Normal University, Shijiazhuang 050016, P. R. China, and Department of Chemistry, Handan College, Handan 056005, P. R. China

A binuclear holmium(III) benzoate 1,10-phenanthroline ternary complex, $[Ho(BA)_3phen]_2$, was synthesized and characterized by elemental analysis, IR and UV spectroscopy, molar conductance, single crystal X-ray diffraction, and thermogravimetric/differential thermogravimetric (TG-DTG) techniques. The crystal of the complex is in a triclinic crystal system, space group $p\bar{1}$ with $a = 10.7162(18)$ Å, $b = 11.845(3)$ Å, $c = 12.227(2)$ Å, $\alpha = 105.141(11)°$, $\beta = 93.845(8)°$, $\gamma = 112.880(5)°$, and $Z = 1$. Each Ho(III) cation in the crystal is eight-coordinated including two O atoms of one chelating bidentate carboxylate group, four O atoms of four bridging bidentate carboxylate groups, and two N atoms of one 1,10-phenanthroline molecule, yielding a distorted square antiprismatic comformation. The thermal analysis of $[Ho(BA)_3phen]_2$ has been performed by simultaneous TG/DSC-FTIR techniques. By the Malek method, SB(*m*,*n*) was defined as a kinetic model for the second-step thermal decomposition. The activation energy E of this step is 296.99 kJ·mol^{-1}, and the pre-exponential factor ln A is 39.99 s^{-1}. The thermodynamic parameters, Gibbs energy ($\Delta G^{\neq}$), enthalpy ($\Delta H^{\neq}$), and entropy ($\Delta S^{\neq}$) of activation, at the peak temperatures were also calculated. The heat capacity of $[Ho(BA)_3phen]_2$ was measured by differential scanning calorimetry (DSC) over the temperature range from (254 to 470) K. In addition, the values of the experimental heat capacities were fitted to a polynomial equation with the least-squares method.

Introduction

Currently, more and more attention has been paid to lanthanide carboxylate complexes for their fascinating structural properties and their potential application as functional materials. Up to now, the studies on their structural and luminescence properties[1−5] have been systematic, and there has been much research on their thermal decomposition.[6−9] However, there are less studies on the thermochemical properties of the rare earth carboxylate complexes. The heat capacity $C_{p,m}$ is a key thermophysical quantity for the material from which other thermodynamic properties such as enthalpy, entropy, and Gibbs energy can be calculated. These parameters are significant for both theoretical and practical purposes.[10,11]

In the present paper, we synthesized and characterized a new lanthanide carboxylate complex $[Ho(BA)_3phen]_2$. The thermal decomposition process of the complex and the evolved gases were discussed, and the nonisothermal kinetics was also established by the Malek method.[12,13] In addition, the heat capacity of the complex was measured over the temperature range from (254 to 470) K.

Experimental Section

Chemicals and Apparatus. All chemicals and solvents were of analytical grade. $HoCl_3·6H_2O$ was prepared by dissolving its oxide in hydrochloric acid and then drying the solution by water-bath heating. Elemental analyses of C, H, and N were carried out on a Vario-EL III elemental analyzer. The metal content was assayed using an ethylenediaminetetraacetic acid (EDTA) titration method. The IR spectra were recorded on a Bruker TENSOR27 spectrometer in the range of (4000 to 400) cm^{-1} using the conventional KBr discs technique at room temperature. The UV spectra were obtained on a Shimadzu 2501 spectrophotometer. The molar conductance was measured with a Shanghai DDS-307 conductometer. The single crystal X-ray diffraction data were obtained by a Saturn724+ diffractometer with graphite-monochromated Mo Kα radiation ($\lambda = 0.71073$ Å) at 93(2) K. The structure was solved by direct methods using the SHELXS-97 program and refined by full-matrix least-squares on F^2 using the SHELXL-97 program.

The thermogravimetric (TG), differential thermogravimetric (DTG), differential scanning calorimetric (DSC), and Fourier transform infrared (FTIR) analyses of the evolved gas of the title complex were conducted using a TG/DSC-FTIR system, which was a Netzsch STA 449 F3 Instrument with a Bruker TENSOR27 Fourier transform infrared spectrometer. About 6 mg of sample was weighed into an open Al_2O_3 crucible, and the furnace temperature was programmed to rise from (303.15 to 1000) K linearly at the rates of (3, 5, 7, 10, and 15) K·min^{-1}, respectively, with nitrogen gas of high purity (≥ 99.999 %) as the carrier gas. The Netzsch STA 449 F3 instrument was linked to the heated gas cell of the FTIR instrument by means of a heated transfer line, and the temperatures of the cell and the transfer line were kept at 473 K.

The heat capacity of the prepared complex was determined using a Netzsch DSC 200 F3 in the temperature range of (254 to 470) K under the linear heating rate of 10 K·min^{-1} using an indirect measurement method. The atmosphere was nitrogen gas with a purity of 99.999 %, and the flow rate was 50 mL·min^{-1}. To verify the reliability of the heat capacity measurement method by DSC,

* Corresponding author. Tel.: +86-31186269386. Fax: +86-31186268405. E-mail address: jjzhang6@126.com.
† Experimental Center, Hebei Normal University.
‡ College of Chemistry & Material Science, Hebei Normal University.
§ Handan College.

10.1021/je100561t
Published on Web 08/17/2010

Table 1. Important IR Absorption Bands for the Ligands and Complex (cm^{-1})

ligands and complex	$\nu_{C=N}$	$\nu_{C=O}$	$\nu_{as(COO^-)}$	$\nu_{s(COO^-)}$	δ_{C-H}		ν_{Ho-O}
phen	1561	−	−	−	854	738	−
HBA	−	1689	−	−			−
$[Ho(BA)_3phen]_2$	1518	−	1617	1424	852	720	426

the heat capacity of the reference standard material sapphire was measured, and the relative deviations of our experimental results were within 0.50 % compared with the recommended values by the National Institute of Standards and Technology (NIST).[14] The baseline, reference, and sample measurements were carried out under the same conditions. The mass of the sample loaded in an aluminum crucible pierced lid was accurately weighed before each heating, and the reference standard substance sapphire mass used was 37.66 mg. Here, the reference and samples were loaded in the same aluminum crucible. The apparatus has an automatic data processing program from which we can obtain the C_p curves of the sample by an indirect measurement method. The sample masses were about 12 mg.

Preparation of the Title Complex. The complex of $[Ho(BA)_3phen]_2$ was prepared by the addition of ethanol solution of the mixed ligands (pH = 6 to 7) of benzoic acid and 1,10-phenanthroline to the $HoCl_3$ aqueous solution under stirring, in which the mole ratio of $HoCl_3 \cdot 6H_2O$, benzoic acid, and 1,10-phenanthroline is 1:3:1. The pH value of the mixed ligand ethanol solution was adjusted with 1 $mol \cdot L^{-1}$ NaOH solution. The reaction mixture was continually stirred for about 8 h at room temperature and then deposited for 12 h. Subsequently, the precipitate was filtered off, washed with 95 % ethanol, and dried in an IR dryer at 373.15 K to a constant mass. The mother liquor was left to stand at room temperature for a few days, and the resulting crystals were selected out and washed with distilled water. The colorless crystals produced were suitable for X-ray diffraction analysis. Elemental analyses for $C_{66}H_{46}N_4O_{12}Ho_2$ (%): calcd: C, 55.94; H, 3.27; N, 3.95; Ho, 23.28; found: C, 56.02;, H, 3.21; N, 3.89; Ho, 23.69.

Results and Discussion

Molar Conductance. The prepared complex was dissolved in dimethyl sulfoxide (DMSO) solution, and its molar conductance was measured with DMSO as a reference. The value is 28.2 $s \cdot cm^2 \cdot mol^{-1}$, indicating that the complex is a nonelectrolyte.[15]

IR Spectra. Table 1 shows the important IR frequencies of the complex and ligands. The band at 1689 cm^{-1}, because of the free COOH group in the benzoic acid, disappears completely in the spectra of the complex, whereas there appear two bands at (1617 and 1424) cm^{-1} that arise from asymmetric and symmetric vibrations of the COO^- group, and the appearance of an absorption band at 426 cm^{-1} is attributed to the ν_{Ho-O}. These changes indicate that the oxygen atoms from the carboxylate group are coordinated to the Ho(III) cation.[16] In addition, $\Delta\nu(COO^-)$ (193 cm^{-1}) of the complex is less than that in sodium salt of benzoic acid (209 cm^{-1}), from which we can infer that the COO^- groups have a bidentate coordination mode with the Ho(III) cation.[17] This result is also consistent with the crystal structure of the complex. The bands of $\nu_{C=N}$ (1561 cm^{-1}), δ_{C-H} [(854 and 738) cm^{-1}] in the spectra of 1,10-phenanthroline are observed to move to lower wavenumbers in the spectra of the complex, suggesting the coordination of the two nitrogen atoms of the neutral ligand to the Ho(III) cation.[18]

UV Spectra. The complex and two ligands were recorded in DMSO solution by UV spectra with DMSO as a reference. The maximum absorbance λ_{max} of the free acid ligand HBA is 256.0 nm with an absorbance A_{max} of 0.02. The main absorption of the complex $[Ho(BA)_3phen]_2$ is 264.20 nm, suggesting that the free acid ligands were coordinated to the metal cation because of a red shift of the absorption peak from the free acid ligands to the complex explained by the formation of a bigger π-conjugated system.[19] Moreover, compared with the complex, the maximum peak of phen at 265.00 nm is similar to that in the complex, indicating that the formation of the coordination bond of Ho−N should have no significant influence on the UV absorption of the phen, which has a similar result for Ln−N in the rare earth complexes with 3,5-dinitrosalicylic acid and 1,10-phenanthroline.[20] However, the absorbance of phen is enhanced from 0.31 to 0.78, which may suggest that a bigger chelate complex is formed.

Table 2. Crystal Data and Structure Refinement for the Complex $[Ho(BA)_3phen]_2$

item	data
empirical formula	$C_{66}H_{46}N_4O_{12}Ho_2$
formula weight	1416.93
temperature	93(2) K
wavelength	0.71073 Å
crystal system, space group	triclinic, $P\bar{1}$
unit cell dimensions	a = 10.7162(18) Å; α = 105.141(11)°
	b = 11.845(3) Å; β = 93.845(8)°
	c = 12.227(2) Å; γ = 112.880(5)°
volume	1355.2(4) $Å^3$
Z, calculated density	1, 1.736 $mg \cdot m^{-3}$
absorption coefficient	2.970 mm^{-1}
$F(000)$	700
crystal size	(0.40 × 0.27 × 0.13) mm
θ range for data collection	3.36° to 27.49°
limiting indices	$-13 \le h \le 13$, $-15 \le k \le 15$, $-15 \le l \le 14$
reflections collected/unique	13690/6132 [$R_{(int)}$ = 0.0264]
completeness to θ = 27.50	98.7 %
absorption correction	semiempirical from equivalents
max. and min transmission	0.6934 and 0.3829
refinement method	full-matrix least-squares on F^2
data/restraints/parameters	6132/2/379
goodness-of-fit on F^2	1.001
final R indices [$I > 2\sigma(I)$]	R_1 = 0.0219, wR_2 = 0.0467
R indices (all data)	R_1 = 0.0250, wR_2 = 0.0478
largest diff. peak and hole	(0.881 and −0.772) $e \cdot Å^{-3}$

Table 3. Selected Bond Lengths [Å] and Angles [deg] for the Complex $[Ho(BA)_3phen]_2$[a]

bond	d, Å	bond	d, Å
Ho(1)−O(6)#1	2.2703(16)	Ho(1)−O(2)#1	2.3167(16)
Ho(1)−O(1)	2.3297(16)	Ho(1)−O(5)	2.3646(16)
Ho(1)−O(3)	2.3658(17)	Ho(1)−O(4)	2.4757(16)
Ho(1)−N(1)	2.534(2)	Ho(1)−N(2)	2.607(2)
angle	ω, deg	angle	ω, deg
O(6)#1−Ho(1)−O(2)#1	73.80(6)	O(6)#1−Ho(1)−O(1)	80.02(6)
O(2)#1−Ho(1)−O(1)	132.93(6)	O(6)#1−Ho(1)−O(5)	126.34(6)
O(2)#1−Ho(1)−O(5)	86.25(6)	O(1)−Ho(1)−O(5)	78.65(6)
O(6)#1−Ho(1)−O(3)	88.45(6)	O(2)#1−Ho(1)−O(3)	86.75(6)
O(1)−Ho(1)−O(3)	131.30(6)	O(5)−Ho(1)−O(3)	140.47(6)
O(6)#1−Ho(1)−O(4)	76.55(6)	O(2)#1−Ho(1)−O(4)	131.01(5)
O(1)−Ho(1)−O(4)	77.10(6)	O(5)−Ho(1)−O(4)	142.51(6)
O(3)−Ho(1)−O(4)	54.21(6)	O(6)#1−Ho(1)−N(1)	144.86(6)
O(2)#1−Ho(1)−N(1)	140.29(6)	O(1)−Ho(1)−N(1)	77.72(6)
O(5)−Ho(1)−N(1)	75.00(6)	O(3)−Ho(1)−N(1)	86.20(6)
O(4)−Ho(1)−N(1)	72.21(6)	O(6)#1−Ho(1)−N(2)	146.87(6)
O(2)#1−Ho(1)−N(2)	76.77(6)	O(1)−Ho(1)−N(2)	132.29(6)
O(5)−Ho(1)−N(2)	65.59(6)	O(3)−Ho(1)−N(2)	74.93(6)
O(4)−Ho(1)−N(2)	113.37(6)	N(1)−Ho(1)−N(2)	63.66(6)

[a] Symmetry transformations used to generate equivalent atoms: #1: $-x + 1$, $-y + 1$, $-z + 1$.

Single-Crystal X-ray Diffraction Studies. Table 2 presents the summary of the unit cell parameters, data collection, and refinement details. The selected bond lengths and angles are listed in Table 3. The binuclear molecular structure of $[Ho(BA)_3phen]_2$ and the detailed coordination sphere around the Ho(III) cation are shown in Figures 1 and 2, respectively.

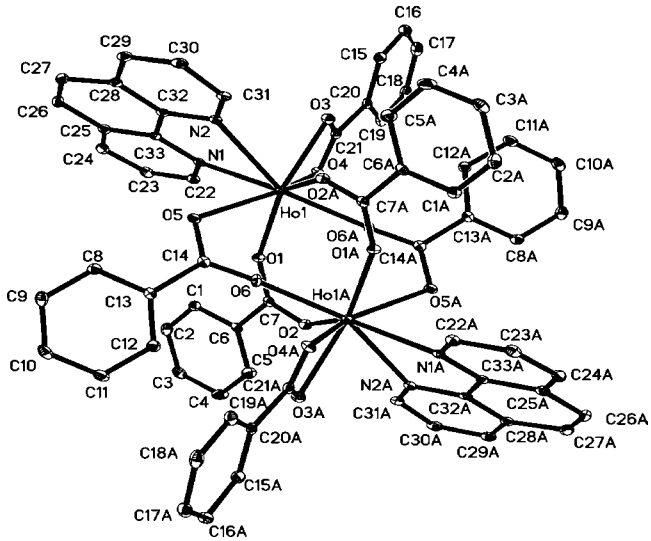

Figure 1. Molecular structure and atom labeling scheme of $[Ho(BA)_3phen]_2$. CCDC 775374 is the number of the Ho(III) complex, which contains the supplementary crystallographic data for this paper. These data can be obtained free of charge from The Cambridge Crystallographic Data Centre via www.ccdc.cam.ac.uk/data_request/cif.

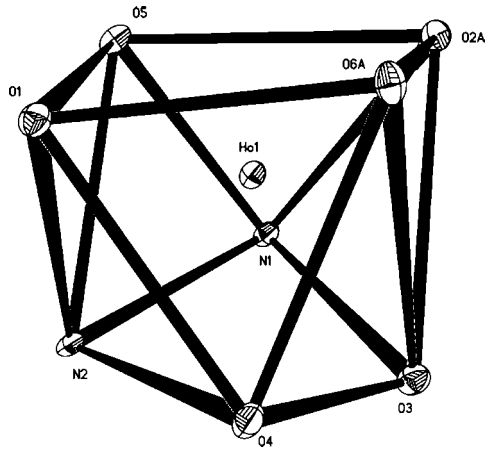

Figure 2. Coordination geometry about the Ho(III) cation.

As shown in Figure 1, two Ho(III) cations are linked by four bridging bidentate carboxylate groups, forming a binuclear complex with a crystallographic inversion center. In the molecular structure, carboxyl groups exhibit a chelating bidentate and bridging bidentate with two kinds of coordination modes. Each Ho(III) cation is coordinated by six oxygen atoms from carboxyl groups and two nitrogen atoms from a phen, yielding a distorted square antiprismatic comformation (in Figure 2), in which atoms O1, O5, O2A, and O6A form the topside face of the square antiprism and the underside face is formed by atoms N1, N2, O3, and O4. The distances of Ho−O range from [2.2703(16) to 2.4757(16)] Å, and its average distance is 2.3538(16) Å. The length of the Ho−N bonds is in the range of [2.534(2) to 2.607(2)] Å with a mean bond length of 2.5705(2) Å. By comparing the crystal structures of serial lanthanide benzoate 1,10-phenanthroline ternary complexes,[1,3,8] both bond lengths of Ln−O and Ln−N are shortened gradually with the atomic number from Eu to Ho, and this may be related to the shorter radius with the increment of atomic number caused by the result of lanthanide contraction. At the same time, we can observe that Ln−O is shorter than Ln−N because of the stronger coordination ability of the oxygen than the nitrogen atom, which indicates that the bond energy of Ln−O is stronger than that of the Ln−N bond. In the thermal decomposition process, the neutral

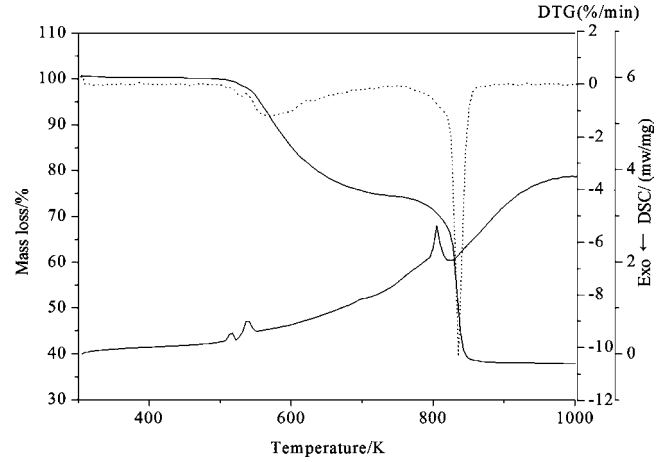

Figure 3. TG, DTG, and DSC curves of the title complex.

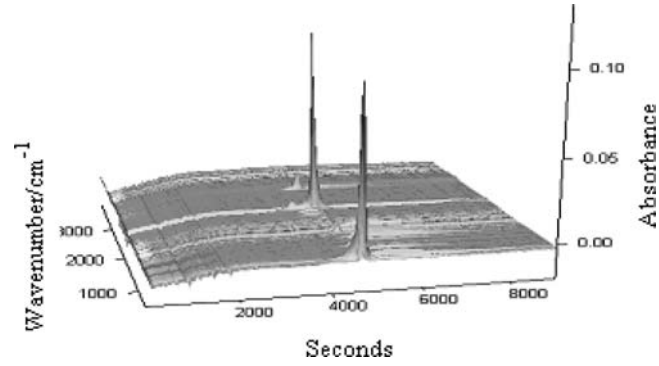

Figure 4. Stacked plot of the FTIR spectra of the evolved gases for the complex as observed in the online TG-FTIR system (heating rate 7 K·min^{-1}, initial mass 6.188 mg).

ligand phen should decompose first, which can also be proved by the thermal analyses.

Thermal Decomposition Process of the Title Complex. TG, DTG, and DSC curves of the title complex at a heating rate of 7 K·min^{-1} under a dynamic N_2 atmosphere are presented in Figure 3 with a good resolution. On the basis of the DTG curve, the thermal decomposition process of the complex can be divided into two main stages, for the splitting of the first two peaks is not obvious. The first stage is from (501.15 to 752.15) K with a mass loss of 25.67 %, which coincides well with the theoretical value of 25.44 % calculated for the loss of 2 mol of phen from the complex. The IR spectra of the residue at 752.15 K shows that the absorption band of C═N at 1518 cm^{-1} disappears, which also indicates that the phen ligands have decomposed. The second stage degradation temperature is in the range of (752.15 to 928.15) K with a mass loss of 36.42 %, and the complex decomposed to a mixture of the carbon and the oxide of holmium. The DSC curve reveals three sharp endothermic peaks. The two continuous peaks between (511.15 and 570.15) K represent the loss of 2 mol of phen from the complex, corresponding to the first two peaks of the DTG curve. The third peak is observed between (804.15 and 865.15) K corresponding to the loss of part of the BA from the $[Ho_2(BA)_6]$.

TG-FTIR Spectra of Gaseous Products. The FTIR spectrum of the gaseous products of the thermal decomposition was obtained for the complex. From Figure 4 below 800 K (that is, 4300 s), there is no characteristic band observed, which may be due to the two steps occurring nearly continuously and the first decomposition step taking place slowly. Heating up to about 846 K, most of the gaseous products are released, and Figure 5 shows the FTIR spectra of these products at two temperatures. The absorption bands

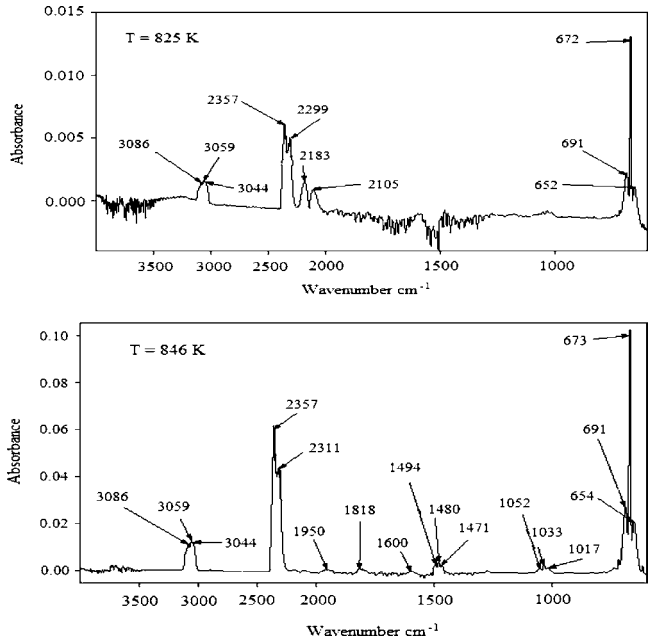

Figure 5. FTIR spectra of the evolved gases for the complex at (825 and 846) K.

attributed to carbon dioxide molecules are situated around (2357 to 2299 and 672) cm^{-1}, with the first corresponding to the stretching asymmetric vibration and the second presenting the deformation vibration of CO_2 molecules. A small amount of carbon monoxide can also be observed, and its molecular vibrations give a detectable double band in the range (2183 to 2105) cm^{-1}.[21] Besides carbon oxides, in the FTIR spectra other gaseous compounds are detected. The absorption peaks at (3086, 3059, and 3044) cm^{-1} are attributed to stretching vibrations of ═CH from evolved aliphatic or aromatic hydrocarbons. The band at 1950 cm^{-1} is connected with the stretching vibrations of C═C═C. The absorption peak at 1818 cm^{-1} is ascribed to the stretching vibration of C═O of a saturated four-membered ring lactone. The characteristic absorption bands at (1600 and 1494) cm^{-1} can be attributed to stretching vibrations of the benzene ring. The bands at (1480 and 1471) cm^{-1} can be attributed to deformation vibration of CH_3 groups or deformation and stretching vibrations of the aromatic ring. Bands in the wavenumber range of 1033 cm^{-1} are observed, corresponding to the C—H bending deformation of the benzene ring or rocking vibrations of CH_3 groups.[22,23] The bands of (1600 and 1052) cm^{-1} can also be considered as deformation vibration of N—H and stretching vibration of C—N. Here, one cannot distinguish among all of the evolved gases because of overlapping (similar wavelengths) in the FTIR spectra. Other diatomic molecules that do not possess a permanent dipole moment are not IR active and therefore cannot be detected using IR absorption.

Heat Capacity of the Title Complex. Three parallel experiments were carried out, and the average results were obtained from the measured values. Experimental molar heat capacities of $[Ho(BA)_3phen]_2$ measured by DSC from (254 to 470) K are listed in Table 4 and plotted in Figure 6. It can be seen that the $C_{p,m}$ of the complex increases with temperature and no endothermic or exothermic peaks exist in the range of the measured temperature, which indicates that no phase change and thermal anomaly occurred and the sample is thermostable. The average values of the experimental heat capacities were fitted to the following polynomial in reduced temperature (x) by means of the least-squares method.[24,25] The equation is the following:

Table 4. Experimental Molar Heat Capacities of $[Ho(BA)_3phen]_2$ (M = 1416.93 g·mol^{-1})

T/K	$C_{p,m}$/J·K^{-1}·mol^{-1}	T/K	$C_{p,m}$/J·K^{-1}·mol^{-1}	T/K	$C_{p,m}$/J·K^{-1}·mol^{-1}
254	1052.75	329	1362.95	401	1614.72
257	1065.48	332	1372.27	404	1626.57
260	1078.44	335	1379.86	407	1639.20
263	1091.83	338	1390.18	410	1649.43
266	1104.16	341	1399.39	413	1660.65
269	1118.91	344	1408.90	416	1668.84
272	1130.49	347	1416.17	419	1680.67
275	1143.31	350	1425.77	422	1693.51
278	1156.29	353	1437.66	425	1702.85
281	1167.20	356	1447.90	428	1716.10
284	1178.34	359	1459.13	431	1730.62
287	1190.85	362	1468.65	434	1742.02
290	1203.07	365	1482.95	437	1750.05
293	1217.81	368	1493.45	440	1766.99
296	1229.93	371	1497.06	443	1778.87
299	1243.89	374	1516.17	446	1789.19
302	1260.31	377	1526.29	449	1798.95
305	1273.71	380	1538.39	452	1805.93
308	1285.40	383	1550.12	455	1815.59
311	1297.43	386	1558.87	458	1822.23
314	1308.47	389	1570.78	461	1829.48
317	1321.23	392	1579.83	464	1837.56
320	1333.76	395	1593.56	467	1844.86
323	1340.98	398	1605.30	470	1855.04
326	1347.33				

$$C_{p,m}/J\cdot mol^{-1}\cdot K^{-1} = 1473 + 369.63x + 26.161x^2 + 103.6x^3 - 47.695x^4 - 74.217x^5$$

where x is the reduced temperature, $x = [T - (T_{max} + T_{min})/2]/[(T_{max} - T_{min})/2]$, T is the experimental temperature, and T_{max} and T_{min} are the respective upper limit (470 K) and lower limit (254 K) in the above measured temperature region. The coefficient of determination of the fitting is $R^2 = 0.9998$.

Kinetics of the Second Decomposition Stage. The Malek method[12,13] was applied to study the kinetics of the second thermal decomposition process of $[Ho(BA)_3phen]_2$. The activation energy E is the most important factor in the determination of the function $f(\alpha)$ by using the Malek method. Here we first obtained the activation energy E of the second decomposition step by an integral isoconversional nonlinear method (NL-INT method)[26] and the Madhusudanan−Krishnan−Ninan method (MKN method)[27] with the condition of not involving the kinetic function. The methods are as follows:

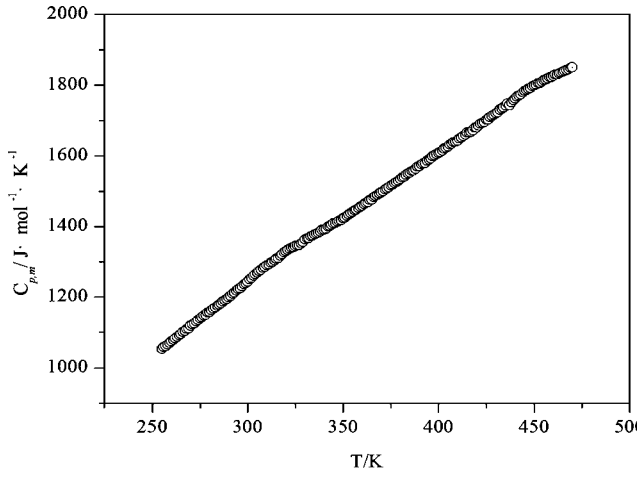

Figure 6. Relationship of molar heat capacities of $[Ho(BA)_3phen]_2$ varying with temperature.

Table 5. Experimental and Calculated Data by the Integral Isoconversional Nonlinear Method (NL-INT) and Madhusudanan−Krishnan−Ninan Method (MKN)

	temperature/K					E/(kJ·mol^{-1})		
α	3 K·min^{-1}	5 K·min^{-1}	7 K·min^{-1}	10 K·min^{-1}	15 K·min^{-1}	NL-INT	MKN	r
0.050	780.65	791.15	792.25	796.75	812.05	261.760	261.830	0.9538
0.075	789.35	799.75	801.45	805.25	818.85	289.070	289.140	0.9637
0.100	795.55	805.85	808.75	812.25	824.55	301.560	301.630	0.9765
0.125	800.75	810.75	814.35	817.65	829.15	312.390	312.460	0.9822
0.150	804.95	815.05	819.15	822.25	833.25	316.880	316.950	0.9851
0.175	808.45	819.05	822.85	826.15	836.95	317.830	317.910	0.9850
0.200	811.65	822.15	826.45	829.25	839.95	322.310	322.390	0.9850
0.225	814.25	824.75	829.25	831.75	842.35	326.490	326.570	0.9844
0.250	816.05	826.55	831.35	833.65	844.15	327.470	327.550	0.9846
0.275	816.95	827.75	832.95	835.15	845.65	320.660	320.740	0.9848
0.300	817.75	828.55	833.85	836.35	846.75	317.730	317.80	0.9868
0.325	818.35	829.25	834.75	837.35	847.65	314.470	314.540	0.9877
0.350	818.85	829.85	835.45	838.25	848.45	311.340	311.40	0.9888
0.375	819.25	830.35	836.05	838.95	849.15	308.290	308.350	0.9893
0.400	819.75	830.85	836.55	839.65	849.75	307.480	307.530	0.9902
0.425	820.15	831.25	837.05	840.25	850.35	305.500	305.560	0.9908
0.450	820.55	831.65	837.45	840.85	850.95	303.700	303.750	0.9916
0.475	820.95	831.95	837.85	841.45	851.45	302.570	302.620	0.9926
0.500	821.35	832.35	838.15	841.95	851.95	301.930	301.980	0.9932
0.525	821.65	832.75	838.55	842.45	852.45	300.130	300.180	0.9934
0.550	821.95	833.05	838.85	842.95	852.95	298.250	298.30	0.9940
0.575	822.35	833.35	839.25	843.45	853.45	297.280	297.320	0.9945
0.600	822.65	833.75	839.55	844.05	853.95	295.410	295.460	0.9951
0.625	823.05	834.05	839.95	844.55	854.45	294.430	294.480	0.9956
0.650	823.45	834.45	840.35	845.15	854.95	293.460	293.500	0.9961
0.675	823.85	834.85	840.85	845.75	855.55	291.580	291.620	0.9965
0.700	824.35	835.35	841.45	846.35	856.15	290.820	290.870	0.9965
0.725	824.95	835.95	842.15	847.05	856.85	290.140	290.180	0.9966
0.750	825.45	836.45	842.75	847.75	857.65	287.590	287.630	0.9969
0.775	826.05	837.05	843.45	848.55	858.45	285.920	285.960	0.9971
0.800	826.75	837.55	844.25	849.55	859.55	282.080	281.560	0.9977
0.825	827.45	838.25	845.25	850.65	860.75	277.710	277.750	0.9980
0.850	828.15	839.05	846.35	851.85	862.15	272.030	272.070	0.9980
0.875	829.05	840.05	847.65	853.35	864.15	263.840	263.880	0.9980
0.900	830.25	841.15	849.15	855.25	866.55	255.020	255.070	0.9982
0.925	831.95	842.65	851.05	857.55	869.65	245.770	245.820	0.9977
						[a]297.010	[a]296.970	

[a] Average value of E.

NL-INT method:

$$\Omega_{1I}(E_\alpha) = \min \left| \sum_{i=1}^{n} \sum_{j \neq i}^{n} \frac{\beta_j \cdot I(E_\alpha, T_{\alpha,i})}{\beta_i \cdot I(E_\alpha, T_{\alpha,j})} - n(n-1) \right| \quad (1)$$

where the integral form of $I(E_\alpha,T_\alpha)$ is the Senum−Yang approximate calculation

$$I_{SY\text{-}3}(E,T) = \left[Te^{-u}\left(\frac{u^2 + 10u + 18}{u^3 + 12u^2 + 36u + 24} \right) \right] \qquad u = E/RT$$

MKN method:

$$\ln\left[\frac{G(\alpha)}{T^{1.921503}}\right] = \left[\ln\frac{AE}{\beta R} + 3.772050 - 1.921503 \ln E\right] - 0.120394(E/T) \quad (2)$$

Equation 2 is changed to

$$\ln\left[\frac{\beta}{T^{1.921503}}\right] = \left[\ln\frac{AE}{RG(\alpha)} + 3.772050 - 1.921503 \ln E\right] - 0.120394(E/T) \quad (3)$$

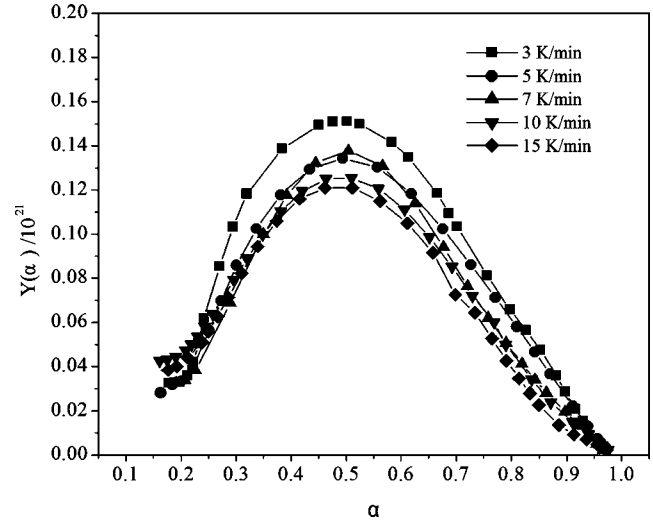

Figure 7. Relationship of $Y(\alpha)$ and α at various heating rates for the second-step decomposition.

The values of the activation energy calculated by eqs 1 and 3 are listed in Table 5. It can be observed that the values calculated by the two methods are in remarkable agreement with each other. The average value of E 296.99 kJ·mol^{-1} was used to calculate the defined function $Y(\alpha)$ and $Z(\alpha)$. The needed experimental data of T, α, and dα/dt are obtained from the TG-DTG curves. The values of $Y(\alpha)$ and $Z(\alpha)$ can be obtained by the substitution of

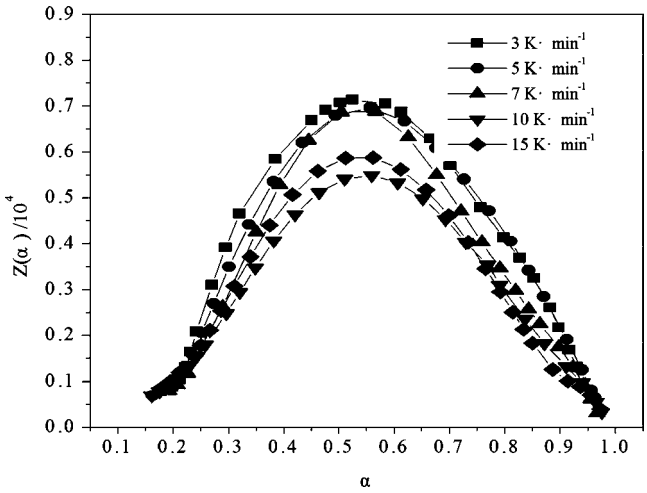

Figure 8. Relationship of $Z(\alpha)$ and α at various heating rates for the second-step decomposition.

experimental data and activation energy E into the following equations:[12]

$$Y(\alpha) = (d\alpha/dt)e^{x} \quad (4)$$

$$Z(\alpha) = \prod(x)(d\alpha/dt)T/\beta \quad (5)$$

where $x = E/RT$ and $\prod(x) = (x^3 + 18x^2 + 88x + 96)/(x^4 + 20x^3 + 120x^2 + 240x + 120)$, which is the expression of the temperature integral. Figures 7 and 8 show the respective curves of the relationship of $Y(\alpha)$ and $Z(\alpha)$ with α at different heating rates. From the two figures, it can be seen that both $Y(\alpha)$ and $Z(\alpha)$ have a clear maximum when α is more than zero. $Y(\alpha)$ indicates that the kinetic model of the second thermal decomposition step of the title complex is JMA($n > 1$) or SM(m,n), while the $Z(\alpha)$ value coincides with the fact that this function has a maximum at α_p^{∞} for all kinetic models summarized in the literature.[12] The Mathematica 4.1 software was used to fit the curves of $Y(\alpha)-\alpha$ and $Z(\alpha)-\alpha$ to obtain the accurate values of α_m and α_p^{∞}, at which function $Y(\alpha)$ and $Z(\alpha)$ have their maxima, respectively. It is found that the equations obtained by a six time fitting are the most accurate.

Table 6. Characteristic Feature of the Functions $Y(\alpha)$ and $Z(\alpha)$

β / K·min^{-1}	shape of the curves	α_m	α_p^{∞}	α_p
3	convex	0.4656	0.5161	0.5394
5	convex	0.4868	0.5384	0.5440
7	convex	0.4927	0.5330	0.5130
10	convex	0.4920	0.5484	0.5298
15	convex	0.4852	0.5375	0.5320

The values of α_m and α_p^{∞} at serial heating rates can be obtained by the derivation of the fitted equations listed in Scheme 1, and Table 6 presents the calculated results. It can be seen from Table 6 that $0 < \alpha_m < \alpha_p$ and the values of α_p^{∞} are not equal to 0.633 at various heating rates. In combination with Figure 4 from Malek,[12] the matched kinetic model of the second thermal decomposition step can be determined to be SB($m.n$). Furthermore, the kinetic exponents m and n and the pre-exponential factor A were calculated by the following equations:[12]

$$\ln[(d\alpha/dt)e^{x}] = \ln A + n \ln[\alpha_p(1 - \alpha)] \quad (6)$$

$$m = pn \quad (7)$$

$$p = \alpha_m(1 - \alpha_m) \quad (8)$$

$$A = -\beta x_p \exp(x_p)/[Tpf'(\alpha_p)] \quad (9)$$

where $f'(\alpha_p) = (df(\alpha_p)/d\alpha)$ and the results are given in Table 7.

Scheme 1

β=3 K·min^{-1}

$Y(\alpha) = 0.496364-7.695\alpha+48.0221\alpha^2-129.791\alpha^3+179.901\alpha^4-126.118\alpha^5+35.4824\alpha^6$

$Z(\alpha) = 1.60301-26.3569\alpha+156\alpha^2-401.368\alpha^3+527.669\alpha^4-351.833\alpha^5+94.2977\alpha^6$

β=5 K·min^{-1}

$Y(\alpha) = 0.353062-5.26817\alpha+30.0764\alpha^2-75.4208\alpha^3+96.2435\alpha^4-62.1943\alpha^5+16.2108\alpha^6$

$Z(\alpha) = 1.37697-20.8808\alpha+115.397\alpha^2-272.296\alpha^3+325.846\alpha^4-197.904\alpha^5+48.4294\alpha^6$

β=7 K·min^{-1}

$Y(\alpha) = 0.358136-4.59739\alpha+22.1577\alpha^2-43.7209\alpha^3+38.7964\alpha^4-13.9035\alpha^5+0.900911\alpha^6$

$Z(\alpha) = 0.860212-10.4084\alpha+39.4226\alpha^2-20.9265\alpha^3-87.8757\alpha^4+131.286\alpha^5-52.4374\alpha^6$

β=10 K·min^{-1}

$Y(\alpha) = 0.256324-3.26421\alpha+17.1594\alpha^2-37.8585\alpha^3+40.9558\alpha^4-22.1273\alpha^5+4.87938\alpha^6$

$Z(\alpha) =0.459554-6.04958\alpha+28.4856\alpha^2-37.3326\alpha^3+0.0086052\alpha^4+27.0874\alpha^5-12.6572\alpha^6$

β=15 K·min^{-1}

$Y(\alpha) = 0.338687-4.58252\alpha+24.8078\alpha^2-59.6394\alpha^3+73.5866\alpha^4-46.8713\alpha^5+123735\alpha^6$

$Z(\alpha) = 1.1922-17.0885\alpha+92.0787\alpha^2-215.787\alpha^3+265.115\alpha^4-174.084\alpha^5+48.6874\alpha^6$

Table 7. Kinetic Parameters and Kinetic Model

β / K·min^{-1}	kinetic model	m	n	ln A / s^{-1}	E / kJ·mol^{-1}
3	SB	0.4452	0.5110	39.46	296.99
5	SB	0.7823	0.8248	39.56	
7	SB	0.8681	0.8748	40.93	
10	SB	0.7879	0.8135	40.15	
15	SB	0.8696	0.9226	39.84	
				39.99[a]	

[a] Average value of ln A.

Table 8. Thermodynamic Parameters of the Complex

β / K·min^{-1}	$\Delta G^{\neq}$ / kJ·mol^{-1}	$\Delta H^{\neq}$ / kJ·mol^{-1}	$\Delta S^{\neq}$ / J·mol^{-1}·K^{-1}	T_p / K
3	235.57	290.16	66.42	821.85
5	234.15	290.07	67.14	832.75
7	224.24	290.02	78.48	838.25
10	229.36	289.98	71.95	842.55
15	230.84	287.90	69.27	852.55
average value	230.83	289.63	70.65	

The thermodynamic parameters of activation can be calculated from the equations:[28,29]

$$A \exp(E/RT) = \nu \exp(-\Delta G^{\neq}/RT) \quad (10)$$

$$\Delta H^{\neq} = E - RT \quad (11)$$

$$\Delta G^{\neq} = \Delta H^{\neq} - T\Delta S^{\neq} \quad (12)$$

where ν is the Einstein vibration frequency, $\nu = k_B T/h$ (k_B and h are Boltzmann and Planck constants, respectively), $\Delta G^{\neq}$ the Gibbs energy of activation, $\Delta H^{\neq}$ the enthalpy of activation, and $\Delta S^{\neq}$ the entropy of activation. The values of three thermodynamic parameters at the peak temperature obtained on the basis of above eqs 10 to 12 are summarized in Table 8.

From Table 8, it can be seen that the $\Delta G^{\neq} > 0$ of the compex indicates that the second decomposition reaction is not spontaneous. In addition, $\Delta H^{\neq} > 0$ suggests that the reaction is endothermic, which is agreement with the third endothermic peak of the DSC curve. Moreover, the average value of the activation energy E, 296.99 kJ·mol^{-1}, in Table 7 demonstrates that the reaction rate of the second step thermal decomposition reaction is slow, which can be explained by the influence of activation energy on the reaction rate: the greater activation energy, the slower reaction rate.[30]

Conclusion

In summary, the title complex has been successfully synthesized, and the crystal structure was determined by single crystal X-ray diffraction. The Ho(III) cation is eight-coordinated with a distorted square antiprism coordination polyhedron. The thermal behavior and the gaseous products of thermal decomposition of the complex are determined in detail by TG/DSC-FTIR. The two organic ligands may be released as CO_2, CO, C_6H_6, and $C_3H_4O_2$, as well as some aliphatic amines and hydrocarbons. The nonisothermal thermal decomposition kinetics of the second step of the complex are studied. The Malek method was used to identify the most probable kinetic model SB(m,n). The activation energy E of this step is 296.99 kJ·mol^{-1}, and the pre-exponential factor ln A is 39.99 s^{-1}. The thermodynamic parameters $\Delta G^{\neq}$, $\Delta H^{\neq}$, and $\Delta S^{\neq}$ of activation at the peak temperature are 230.83 kJ·mol^{-1}, 289.63 kJ·mol^{-1}, and 70.65 J·mol^{-1}·K^{-1}, respectively. Heat capacities of the complex $[Ho(BA)_3phen]_2$ were measured by a differential scanning calorimeter over the temperature range from (254 to 470) K, and the values of experimental heat capacities were fitted to a polynomial equation $C_{p,m}/J \cdot mol^{-1} \cdot K^{-1} = 1473 + 369.63x + 26.161x^2 + 103.6x^3 - 47.695x^4 - 74.217x^5$ with a least-squares method.

Literature Cited

(1) Zhang, Y.; Jin, L. P.; Lu, S. Z. Crystal Structure and Luminescence of Eu(BA)$_3$phen Complex. *J. Chin. Rare Earth Soc.* **1998**, *16* (1), 5–8.

(2) Ye, H. M.; Ren, N.; Zhang, J. J.; Sun, S. J.; Wang, J. F. Crystal Structures, Luminescent and Thermal Properties of a New Series of Lanthanide Complexes with 4-Ethylbenzoic Acid. *New J. Chem.* **2010**, *34* (3), 533–540.

(3) Wang, R. F.; Wang, S. P.; Shi, S. K.; Zhang, J. J. Crystal structure and properties of a terbium benzoate complex with 1,10-phenanthroline. *Chin J. Struct. Chem.* **2004**, *23* (11), 1300–1304.

(4) Sun, S. J.; Ren, N.; Zhang, J. J.; Ye, H. M.; Wang, J. F. Synthesis, Crystal Structure, and Thermal Decomposition Kinetics of the Complex of Ho 2,4-Dichlorobenzoic Acid and 2,2′-Bipyridine. *J. Chem. Eng. Data*, **2010**, *55*, 2458–2462.

(5) Yang, Y. T.; Zhang, S. Y. Study of the columinescence effect of lanthanide ternary complexes with benzoic acid and phenantroline. *Spectrosc. Lett.* **2004**, *37* (1), 1–10.

(6) Zhang, J. J.; Ren, N.; Wang, Y. J.; Xu, X. L.; Wang, R. F.; Wang, S. P. Synthesis, crystal structure and thermal decomposition mechanism of a samarium *o*-chlorobenzoate complex with 1,10-phenanthroline. *J. Braz. Chem. Soc.* **2006**, *17* (7), 1355–1359.

(7) Xu, L. J.; Wang, S. P.; Wang, R. F.; Zhang, J. J. Synthesis, structures and properties of ternary rare earth complexes with fluorobenzoic acid and 1,10-phenanthroline. *J. Coord. Chem.* **2006**, *61* (2), 237–250.

(8) Xu, S. L.; Zhang, J. J.; Ren, N.; Zhang, H. Y.; Hu, R. S. Preparation, Crystal Structure and Thermal Decomposition Process of Dysprosium Benzoate Complex with 1,10-Phenanthroline. *Chin J. Struct. Chem.* **2008**, *27* (2), 233–237.

(9) Zhang, H. Y.; Zhang, J. J.; Ren, N.; Xu, S. L.; Zhang, Y. H.; Tian, L.; Song, H. H. Synthesis, characterization and thermal decomposition kinetics of Sm(III)complex with 2,4-dichlorobenzoate and 2,2′-bipyridine. *J. Alloys Compd.* **2008**, *466*, 281–286.

(10) Shi, Q.; Tan, Z. C.; Di, Y. Y.; Tong, B.; Li, Y. S.; Wang, S. X. Thermal analysis and calorimetric study of 4-dimethylaminopyridine. *J. Chem. Eng. Data* **2007**, *52* (3), 941–947.

(11) Tong, B.; Tan, Z. C.; Shi, Q.; Li, Y. S.; Yue, D. T.; Wang, S. X. Thermodynamic investigation of several natural polyols (I): Heat capacities and thermodynamic properties of xylitol. *Thermochim. Acta* **2007**, *45*, 20–26.

(12) Malek, J. The kinetic analysis of non-isothermal data. *Thermochim. Acta* **1992**, *200*, 257–259.

(13) Malek, J.; Smrcka, V. The kinetic analysis of the crystallization processes in glasses. *Thermochim. Acta* **1991**, *186*, 153–169.

(14) Archer, D. G. Thermodynamic properties of synthetic sapphire (α-Al_2O_3), standard reference material 720 and the effect of temperature-scale differences on thermodynamic properties. *J. Phys. Chem. Ref. Data* **1993**, *22*, 1441–1453.

(15) Geary, W. J. The use of conductivity measurements in organic solvents for the characterisation of coordination compounds. *Coord. Chem. Rev.* **1971**, *7*, 81–122.

(16) Shi, Y. Z.; Sun, X. Z.; Jiang, Y. H., *Spectra and Chemical Identification of Organic Compounds*, Science and Technology Press, Nanjing, 1988,p 98 (in Chinese).

(17) Brown, L. M.; Mazadiyasni, K. S. Synthesis and some properties of yttrium and lanthanide isopropoxides. *Inorg. Chem.* **1970**, *9* (12), 2783–2786.

(18) Bai, G. B.; Chen, G. D.; Wang, Z. M.; Yuan, L.; Kang, Z. W.; Gao, J. Z. Synthesis and Characterization of Ln(III)-Glycine-1,10-Phenathroline Ternary Chelates. *Chin. J. Inorg. Chem* **1988**, *2*, 32–41.

(19) An, B. L.; Gong, M. L.; Li, M. X.; Zhang, J. M. Synthesis, Structure and Luminescence Properties of Samarium(III) and Dysprosium(III) Complexes with a New Tridentate Organic Ligand. *J. Mol. Struct.* **2004**, *687*, 1–6.

(20) Wang, L. F.; Wu, J. G.; Peng, Z. R.; Ran, W.; Yan, G. H. Study on Ternary Complexes of Rare Earth Elements.IV.Syntheses and Properties of Ternary Complexes of Rare Earth Elements with 3,5-Dinitrosalicylic Acid and Phenanthroline. *Chin. J. Inorg. Chem.* **1990**, *6* (2), 141–146.

(21) Sikorska-Iwan, M.; Modzelewska-Banachiewicz, B. Thermal behaviour of 1,2,4,-triazole and 1,2,4-triazine derivatives. *J. Therm. Anal. Calorim.* **2005**, *81*, 119–123.
(22) Shimanouchi, T. *Tables of Molecular Vibrational Frequencies Consolidated*, Vol. I; National Bureau of Standards: Gaithersburg, MD, 1972; pp 1−160.
(23) Lyszczek, R. Thermal and spectroscopic investigations of new lanthanide complexes with 1,2,4-benzentricarboxylic acid. *J. Therm. Anal. Calorim.* **2007**, *90*, 533–539.
(24) Guo, J. P.; Liu, B. P.; Lv, X. C.; Tan, Z. C.; Tong, B.; Shi, Q.; Wang, D. F. Molar heat capacities, thermodynamic properties, and thermal stability of trans-4-(Aminomethyl)cyclohexanecarboxylic acid. *J. Chem. Eng. Data* **2007**, *52*, 1678–1680.
(25) Wang, M. H.; Tan, Z. C.; Sun, X. H.; Zhang, H. T.; Liu, B. P.; Sun, L. X.; Zhang, T. Determination of Heat Capacities and Thermodynamic Properties of 2-(Chloromethylthio)benzothiazole by an Adiabatic Calorimeter. *J. Chem. Eng. Data* **2005**, *50*, 270–273.
(26) Vyazovkin, S.; Dollimore, D. Linear and Nonlinear Procedures in Isoconversional Computations of the Activation Energy of Nonisothermal Reactions in Solids. *J. Chem. Inf. Comput. Sci.* **1996**, *36*, 42–45.
(27) Madhusudanan, P. M.; Krishnan, K.; Ninan, K. N. New approximation for the p(*x*) function in the evaluation of non-isothermal kinetic data. *Thermochim. Acta* **1986**, *97*, 189–201.
(28) Straszko, J.; Olstak-Humienik, M.; Mozejko, J. Kinetics of Thermal Decomposition of $ZnSO_4 \cdot 7H_2O$. *Thermochim. Acta* **1997**, *292*, 145–150.
(29) Olstak-Humienik, M.; Mozejko, J. Thermodynamic Functions of Activated Complexes Created in Thermal Decomposition Processes of Sulphates. *Thermochim. Acta* **2000**, *344*, 73–79.
(30) Fu, X. C.; Chen, R. H. *Physical Chemistry*, Part 2 (in Chinese); Peoples Education Press: Beijing, 1979; p 214.

Received for review May 27, 2010. Accepted August 7, 2010. This project was supported by the National Natural Science Foundation of China (No. 20773034), the Natural Science Foundation of Hebei Province (No. B2007000237, No. E2009000307), and the Education Department Scientific Research Fund from Hebei Province (2008469).

JE100561T